isvr Institute of Sound and Vibration Research

Estimation of Acoustic Source Strength by Inverse Methods: Part III: Experiments

S.H. Yoon and P.A. Nelson

ISVR Technical Report No 280

October 1998

University of Southampton

SCIENTIFIC PUBLICATIONS BY THE ISVR

Technical Reports are published to promote timely dissemination of research results by ISVR personnel. This medium permits more detailed presentation than is usually acceptable for scientific journals. Responsibility for both the content and any opinions expressed rests entirely with the author(s).

Technical Memoranda are produced to enable the early or preliminary release of information by ISVR personnel where such release is deemed to the appropriate. Information contained in these memoranda may be incomplete, or form part of a continuing programme; this should be borne in mind when using or quoting from these documents.

Contract Reports are produced to record the results of scientific work carried out for sponsors, under contract. The ISVR treats these reports as confidential to sponsors and does not make them available for general circulation. Individual sponsors may, however, authorize subsequent release of the material.

UNIVERSITY OF SOUTHAMPTON

INSTITUTE OF SOUND AND VIBRATION RESEARCH

FLUID DYNAMICS AND ACOUSTICS GROUP

Estimation of Acoustic Source Strength by Inverse Methods: Part III: Experiments

by

S H Yoon and P A Nelson

ISVR Technical Report No. 280

October 1998

Authorized for issue by
Professor P A Nelson
Group Chairman

CONTENTS

FIGURES

Figure 14. Condition number $\kappa(\mathbf{H}^{\mathrm{H}}\mathbf{H})$ of the model of Figure 13.

Figure 15. A comparison of the directly measured (black) and reconstructed (by the least squares solution, grey) volume velocity (per unit ampere) auto-spectra of sources (a) 1, (b) 3 and cross-spectra between sources 1 and 3 ((c) magnitude, (d) phase) for the model of Figure 13.

Figure 16. A geometrical arrangement of the plate system discretised into 16 volume velocity sources and 16 microphones.

Figure 17. Condition number $\kappa(\mathbf{H}^{\mathrm{H}}\mathbf{H})$ of the model of Figure 16.

Figure 18. A comparison of the directly measured (black) and reconstructed (by the simple least squares solution, grey) volume velocity (per unit ampere) auto-spectra of sources (a) 1, (b) 11 and cross-spectra between sources 1 and 11 ((c) magnitude, (d) phase) for the model of Figure 16.

Figure 19. Regularisation parameters for the model of Figure 13: β_{qq} (black) and β_{GCV} (grey). $a=L_x/4$, $L_x=0.38$m.

Figure 20. Condition numbers for the model of Figure 13: $\kappa(\mathbf{H}^{\mathrm{H}}\mathbf{H})$ (thick black), $\kappa(\mathbf{H}^{\mathrm{H}}\mathbf{H}+\beta_{qq}\mathbf{I})$ (thin black) and $\kappa(\mathbf{H}^{\mathrm{H}}\mathbf{H}+\beta_{\mathrm{GCV}}\mathbf{I})$ (grey). $a=L_x/4$, $L_x=0.38$m.

Figure 21. Volume velocity (per unit ampere) auto-spectra of sources (a) 1, (b) 3: desired (thick black), unregularised (thin grey), regularised by β_{qq} (thin black), regularised by β_{GCV} (thick grey). (c) Phase of cross-spectra between sources 1 and 3 for the model of Figure 13.

Figure 22. Regularisation parameters for the model of Figure 16: β_{qq} (black) and β_{GCV} (grey). $a=L_x/8$, $L_x=0.38$m.

Figure 23. Condition numbers for the model of Figure 16: $\kappa(\mathbf{H}^{\mathrm{H}}\mathbf{H})$ (thick black), $\kappa(\mathbf{H}^{\mathrm{H}}\mathbf{H}+\beta_{qq}\mathbf{I})$ (thin black) and $\kappa(\mathbf{H}^{\mathrm{H}}\mathbf{H}+\beta_{\mathrm{GCV}}\mathbf{I})$ (grey). $a=L_x/8$, $L_x=0.38$m.

Figure 24. Volume velocity (per unit ampere) auto-spectra of sources (a) 1, (b) 11: desired (thick black), unregularised (thin grey), regularised by β_{qq} (thin black), regularised by β_{GCV} (thick grey). (c) Phase of cross-spectra between sources 1 and 11 for the model of Figure 16.

Figure 25. Singular values of the matrix $\mathbf{H}$ for the model of Figure 13. $a=L_x/4$, $L_x=0.38$m.

Figure 26. Condition numbers for the model of Figure 13: $\kappa(\mathbf{H})$ (thick black), $\kappa(\mathbf{H}_D)$ (thin black) and $\kappa(\mathbf{H}_V)$ (grey). $a=L_x/4$, $L_x=0.38$m.

Figure 27. Volume velocity (per unit ampere) auto-spectra of sources (a) 1, (b) 3: desired

(thick black), undiscarded (thin grey), reconstructed by $\mathbf{H}_D$ (thin black), reconstructed by $\mathbf{H}_V$ (thick grey). (c) Phase of cross-spectra between sources 1 and 3 for the model of Figure 13.

Figure 28. Singular values of the matrix **H** for the model of Figure 16. $a=L_x/8$, L_x=0.38m.

Figure 29. Condition numbers for the model of Figure 16: $\kappa(\mathbf{H})$ (thick black), $\kappa(\mathbf{H}_D)$ (thin black) and $\kappa(\mathbf{H}_V)$ (grey). $a=L_x/8$, L_x=0.38m.

Figure 30. Volume velocity (per unit ampere) auto-spectra of sources (a) 1, (b) 11: desired (thick black), undiscarded (thin grey), reconstructed by $\mathbf{H}_D$ (thin black), reconstructed by $\mathbf{H}_V$ (thick grey). (c) Phase of cross-spectra between sources 1 and 11 for the model of Figure 16.

ABSTRACT

Experiments on the reconstruction of acoustic source strengths by inverse methods are conducted by using a randomly vibrating simply supported plate mounted in a finite baffle. The acoustic source strength distribution is constructed by using measurements of the radiated pressure field and assumed transfer functions between the elements of the vibrating plate and the acoustic pressure at the measurement positions. The least squares method is used for both well- and ill-conditioned experimental models. Regularisation methods such as Tikhonov regularisation and singular value discarding are employed to enhance the accuracy of reconstruction for the ill-conditioned experimental models. The Tikhonov regularisation parameter and the singular values to be discarded are determined by using the generalised cross-validation technique. These methods are found to enhance considerably the accuracy of source strength reconstruction when the problem is ill-conditioned.

1. INTRODUCTION

In reference [1] we addressed the importance of the proper choice of microphone array geometry when using inverse methods for the reconstruction of acoustic source strength. Methods for choosing regularisation parameters have also been discussed in reference [2] and it has been demonstrated by computer simulation that good results can be achieved even when the inverse problem is ill-conditioned. This report is concerned with the experimental reconstruction of volume velocities of a randomly vibrating simply supported plate mounted in a finite baffle. The report starts with a detailed description of the construction of the simply supported plate and associated experimental approach. Experiments are undertaken for various conditions of the discretisation of the plate, the geometry of microphone array, and the frequency range to be analysed. However, each experiment belongs to one of two types of model: a well-conditioned model or an ill-conditioned model. With the first type of model, we wish to explore how precisely the least squares solution alone is able to reconstruct the volume velocities of the plate. The second type of model is used to investigate the performance of Tikhonov regularisation and singular value discarding in enhancing the reconstruction accuracy. These experiments also show the limitation of the least squares solution for ill-conditioned models. The choice of the regularisation parameter and the singular values to be discarded is made by employing the methods presented in reference [2]. Of those, we are mainly concerned with the effectiveness of the use of generalised cross-validation. Furthermore, regarding the performance of the least squares solution, it will be also useful to refer to reference [3] which presents the results of experiments on the reconstruction of the strengths of two volume velocity sources under various conditions.

2. THEORETICAL BACKGROUND

In order to reconstruct the volume velocities of acoustic sources from the measurement of acoustic pressures, we used the least squares method with minimal norm [1]. The optimally estimated vector of volume velocities is given by

$$\mathbf{q}_o = \{(\mathbf{H}^{\mathrm{H}}\mathbf{H})^{-1}\mathbf{H}^{\mathrm{H}}\}\hat{\mathbf{p}}, \tag{1}$$

and the cross-spectral matrix of volume velocities is

$$\mathbf{S}_{qqo} = \{(\mathbf{H}^{\mathrm{H}}\mathbf{H})^{-1}\mathbf{H}^{\mathrm{H}}\}\mathbf{S}_{\hat{p}\hat{p}}\{(\mathbf{H}^{\mathrm{H}}\mathbf{H})^{-1}\mathbf{H}^{\mathrm{H}}\}^{\mathrm{H}}, \tag{2}$$

where $\mathbf{H}$ is the matrix consisting of the transfer functions relating the vector $\mathbf{q}$ of source strengths to the vector $\mathbf{p}$ of desired acoustic pressures and $\hat{\mathbf{p}}$ and $\mathbf{S}_{\hat{p}\hat{p}}$ are respectively the vector and the cross-spectral matrix of measured acoustic pressures. The superscript $^{\mathrm{H}}$ denotes the Hermitian transpose (complex conjugate transpose). We have also introduced two regularisation methods [1, 2] incorporated with the least squares solution in order to enhance the reconstruction accuracy through improvement of conditioning of the matrices to be inverted. The Tikhonov regularised solution for the volume velocities is given by

$$\mathbf{q}_R = \{(\mathbf{H}^{\mathrm{H}}\mathbf{H} + \beta\mathbf{I})^{-1}\mathbf{H}^{\mathrm{H}}\}\hat{\mathbf{p}}, \tag{3}$$

and the Tikhonov regularised solution for the volume velocity cross-spectra is

$$\mathbf{S}_{qqR} = \{(\mathbf{H}^{\mathrm{H}}\mathbf{H} + \beta\mathbf{I})^{-1}\mathbf{H}^{\mathrm{H}}\}\mathbf{S}_{\hat{p}\hat{p}}\{(\mathbf{H}^{\mathrm{H}}\mathbf{H} + \beta\mathbf{I})^{-1}\mathbf{H}^{\mathrm{H}}\}^{\mathrm{H}}, \tag{4}$$

where β is the regularisation parameter and $\mathbf{I}$ is the identity matrix. The singular value discarded solution of volume velocities is expressed as

$$\mathbf{q}_D = \mathbf{H}_D^{+}\,\hat{\mathbf{p}} = (\mathbf{V}\boldsymbol{\Sigma}_D^{+}\mathbf{U}^{\mathrm{H}})\,\hat{\mathbf{p}}, \tag{5}$$

and the singular value discarded solution of volume velocity cross-spectra is

$$\mathbf{S}_{qqD} = \mathbf{H}_D^{+}\,\mathbf{S}_{\hat{p}\hat{p}}\,(\mathbf{H}_D^{+})^{\mathrm{H}} = (\mathbf{V}\boldsymbol{\Sigma}_D^{+}\mathbf{U}^{\mathrm{H}})\,\mathbf{S}_{\hat{p}\hat{p}}\,(\mathbf{V}\boldsymbol{\Sigma}_D^{+}\mathbf{U}^{\mathrm{H}})^{\mathrm{H}}, \tag{6}$$

where $\mathbf{U}$ and $\mathbf{V}$ are the matrices consisting of the left and right singular vectors of $\mathbf{H}$, Σ_D is the matrix of singular values left after discarding some singular values, the superscript $^+$ denotes the pseudo-inverse and $\mathbf{H}_D = \mathbf{U}\Sigma_D\mathbf{V}^H$.

Since the application of Tikhonov regularisation and singular value discarding perturbs the original matrix to be inverted, it is important to choose carefully the regularisation parameter and the singular values to be discarded [2]. Methods for making this choice are classified into two groups based on whether they require or do not require *a priori* knowledge of either the volume velocity or the noise. We have focused on the use of the generalised cross-validation (GCV) technique which does not require such prior knowledge.

3. EXPERIMENTAL SYSTEM

The experiments were performed on a simply supported plate mounted in a finite baffle. The simply supported boundary condition implies no transverse displacement of the plate edges, although their rotation is permitted. This boundary condition is replicated approximately by the use of shims at the edges of the plate. These are stiff for in-plane motion but flexible for rotation. Figure 1 shows the design of the plate. Fifty holes are tapped for 12BA screws with 0.027m spacing into four edges of an aluminium plate 0.38m long, 0.3m wide and 0.0025m thick. Four shims of 0.004″ thick are fabricated into the four edges of the plate through these tapped holes. In this process, four aluminium strips of 0.001m thick are joined together, since the shims are very thin and are easily torn. In addition, the shims are slotted to adjust the height of the plate. The shape of these slots is designed to ensure that the shims are not crumpled. The aluminium plate and shims fabricated together are fastened to a heavy, very stiff 0.02m thick steel frame. The inside dimension of the steel frame is 0.38m long and 0.3m wide which are precisely the same dimensions as the aluminium plate. Four steel clamping bars 0.01m thick are used to firmly clamp four shims to the four inside surfaces of the steel frame. The dimensions of the steel frame and clamping bars have to be chosen not to produce substructure resonances when the plate is excited.

The fabricated simply supported aluminium plate system consisting of plate, shims, steel frame, and clamping bars is mounted on a medium density fibreboard (MDF) support box. In this process, attention was given to the system design which enabled the most significant reduction of vibration transmission from the steel frame into the MDF box. To this aim, a rubber layer was inserted between the bottom facet of the steel frame and the top facet of the MDF box. After that, the simply supported plate system is placed in the centre of a rigid MDF baffle which is 3m high, 2.8m wide and 0.012m thick. This baffle is used to eliminate significant acoustic interference between the front and rear sound field. At this stage, the dimension of baffle was selected from a consideration of the longest wavelength corresponding to the lowest frequency of interest. In addition, since the thickness of the MDF baffle is small compared with its height and width, it is easy to vibrate even with a small excitation. For this reason, the MDF baffle was reinforced with some square wooden ribs.

Meanwhile, for further reduction of the acoustic interference between the front and rear field of the baffle, an MDF box containing sound absorbent material is made and fastened against the steel main frame via toggle clamps. However, the absorbing box may cause a coupling problem. That is to say, since the space formed by the steel main frame and the absorbing box is an enclosure, the vibrating plate excited by the electromagnetic driver can be an acoustic source exciting the modes of this enclosure. The modes excited can in turn excite the thin aluminium plate and transmit through that to the front acoustic field where acoustic pressures are measured by a microphone array. If this effect is significant, the measurement of acoustic pressures made by the plate vibration itself will be inaccurate. Thus the inside surfaces of the absorbing box are lined with absorbent material. Finally, attention has to be paid to sealing the air gaps existing between the edges of the baffle and the side facets of the MDF supporting box and steel main frame. These gaps were treated so that there is no large vibration transmission among substructures and that the acoustic pressures at the rear side of the baffle do not contaminate those at the front side. To meet these two requirements, these gaps are filled with a sealant.

To generate an acoustic field from the vibration of the plate, it is excited by an electromagnetic driver consisting of a coil wound around a core and a permanent

magnet. The core of the electromagnetic driver is attached to the rear part of the plate which is not coincident with the nodal lines of many structural modes of interest. This electromagnetic driver generates a force by passing an alternating current through the coil. A random noise signal is used to excite the driver and the force generated is input to the plate. In addition, it was ensured that the mechanical input impedance of the driving system did not exceed the impedance of the plate itself below the frequency of interest. This ensures that the dynamic properties of the plate were not changed.

The radiated acoustic field is measured by a microphone array supported by a scanning system (see Figure 2) which adjusts the position of the microphone array. The scanner comprises mainly a frame, a stepper motor and a controller, and operates as follows. Six electret microphones are held on the microphone grippers fixed on the vertical aluminium rods which are designed to enlarge the aperture size of the scanning area. The microphone array locates automatically in the horizontal direction by a stepper motor attached to the 0.09m thick aluminium frame whose dimension is of 1.09m x 1.39m x 0.8m, and manually in the vertical direction by screwing and unscrewing the vertical rods to the aluminium frame. The stepper motor is controlled by the driver which is operated by the control card in connection with the control software, Motion Architect [4] installed in the personal computer. In acquiring pressures by a microphone array and surface velocities by an accelerometer, the current of the coil is also simultaneously obtained to measure the force input by the driving system into the plate. The input force data are used as a normaliser for the pressures and volume velocities. That is to say, the transfer function between the input force and pressures and volume velocities are obtained, instead of pressures and volume velocities themselves. The input force was measured using a force transducer. This, however, caused a problem of significant mechanical input impedance due to its mass (0.02Kg) when compared to the impedance of the plate itself. To resolve this difficulty, a 1Ω resistor is connected with the coil cable in series and the voltage between two ends of the resistor is measured. This voltage is therefore proportional to the current flowing in the coil.

In order to evaluate how well the plate replicates the simply supported boundary condition, the modal parameters such as natural frequencies, mode shapes and damping ratios were extracted via a modal test. This was undertaken by the use of a

small accelerometer and an impact hammer. The experimental natural frequencies can be compared with the theoretical values which are given in reference [5]. Figure 3 compares the experimental and theoretical natural frequencies which were found to be in good agreement. The discrepancy at some natural frequencies is likely to result from the four aluminium strips 0.001m thick and fifty 12BA small screws which change the stiffness and mass of the plate. Also the mode shapes obtained experimentally were compared with those given theoretically [5] and showed reasonably good agreement. The plate can thus be assumed to give a satisfactory replication of the simply supported boundary condition.

4. DIRECT MEASUREMENT OF THE VOLUME VELOCITY OF THE VIBRATING PLATE

To check how successfully the inverse technique reconstructs volume velocities of a vibrating plate, we need data for comparison and these are obtained from direct measurement. Thus, the direct measurement of volume velocity has to be made as accurately as possible. A number of techniques can be employed for measurement of the volume velocity including an accelerometer, a laser doppler velocimeter [6] or more recently a volume velocity transducer [7]. Here we used the accelerometer

If a plate vibrates as like a rigid piston moving in phase, volume velocity q is determined by the expression

$$q = Sv_s \,, \tag{7}$$

where v_s is the local surface velocity measured at any point on the plate and S is the plate area. However, since the plate does not usually show a rigid piston-like motion, the plate should be discretised into a number of small segments. Each segment is regarded as a rigid piston moving in phase. The total volume velocity in this case is determined by the summation of individual contributions of all segments and thus

$$q = \sum_{i=1}^{K} S_i v_{si} \,, \tag{8}$$

where v_{si} and S_i are the volume velocity and area of the ith segment and K is the total number of segments. It is straightforward to measure the volume velocities by use of

the accelerometer. However a major shortcoming the additional loading due to the accelerometer attached to the plate, which can cause a change of the dynamic behaviour of the plate. For this reason, it was necessary to use an accelerometer that was as small as possible. In addition, in order to obtain the volume velocity at high frequencies as accurately as possible, the number of measurement points should be sufficient to avoid spatial aliasing.

The plate is thus divided into 144 (12x12) contiguous small rectangular segments of the same area. Measurements of the surface velocities are then made at the individual centre points of these segments. The volume velocity source consists of the combination of some rectangular segments and then its strength is obtained by the summation of the surface velocities of individual segments multiplied by the area of segment. The measurement of the surface velocities is made by a calibrated accelerometer, which is in turn moved to the centre points of the 144 small rectangular elements. The results of the directly measured volume velocities will be presented in the ensuing sections, where these are compared with those estimated by the inverse technique.

5. EXPERIMENTAL RECONSTRUCTION BY THE LEAST SQUARES METHOD

All experiments have been undertaken in the anechoic chamber (which is of dimensions 9.15m x 9.15m x 7.32m) of the ISVR at the University of Southampton. Since the condition number of the matrix to be inverted plays a crucial role, experiments are conducted for the two main groups which have "small" or "large" condition number (although, strictly speaking, there is not an explicit quantitative scale to distinguish between small and large condition numbers). With the first group, we wish to explore how accurately the simple least squares solution given by equation (2) is able to reconstruct volume velocity sources of the randomly vibrating plate. The second group of experiments are used to investigate how Tikhonov regularisation and singular value discarding improve the reconstruction accuracy.

In this section, we present the results of the first group of experiments. An initial experiment is carried out for the system as shown in Figure 4. The plate is discretised into four volume velocity sources each of which consists of 36 (6x6) of 144 small

segments. Four microphones are placed symmetrically with respect to the sources, setting the microphone-to-microphone distance equal to the source-to-source distance (0.19m in the horizontal direction and 0.15m in the vertical direction). Also the pattern of microphone array is rectangular and the same as that of source array. This geometrical arrangement is selected to make the condition number as small as possible, referring to the behaviour of the condition number of $\mathbf{H}^{H}\mathbf{H}$ described in reference [1]. The condition number for this case is exhibited in Figure 5 and is between 50-300, decreasing as frequency increases. In the experiment using this model, the frequency to be analysed is limited to 500Hz. This is because the discretised individual rectangular elements are regarded as equivalent point monopole sources and therefore the requirement of the condition $ka<<1$ has to be met (a is the typical dimension of a source element, here $a=L_x/4=0.38/4=0.095$m). Some of the reconstructed magnitudes and phases of acoustic source strength auto- and cross-spectra are presented in Figure 6. They are in very good agreement with the directly measured values.

The next experiment has been conducted for the plate model discretised into 16 volume velocity sources as shown in Figure 7. Each volume velocity source of this model is clearly smaller than that of the preceding experimental model. In this case, the frequency to be analysed can be expanded to 1000Hz, based on $ka<<1$ (here $a=L_x/8=0.38/8=0.0475$m). Since the source-to-source distance becomes smaller (i.e., 0.095m in the horizontal direction and 0.075m in the vertical direction), from the viewpoint of conditioning, the microphone-to-microphone distance is also reduced (i.e., 0.095m in the horizontal direction and 0.075m in the vertical direction). Additionally, the 16 microphone array plane is put close to the source array plane at distance of 0.046m (and, of course, the microphone array is placed symmetrically with respect to the source array). Such a placement makes the condition number below 300 (see Figure 8). Note that this condition number is very similar to that of the model of Figure 4 (4 sources and 4 microphones) in spite of the use of more sources and microphones. However, this may give rise to nontrivial acoustical reflections because the microphone scanner (refer to Figure 2) located close to the plate. Hence, attention should be given to the trade-off between the condition number and accurate measurement of acoustic pressures when the geometrical arrangement of microphones

is made. The results of Figure 9 compare the reconstructed and directly measured volume velocities for this experimental model. The reconstructed values follow well the overall trend of the values measured directly up to 1000Hz. However, the results show a more noisy shape than previously (compare Figure 9 with Figure 6). This is, as expected, caused by acoustical reflection from the microphone scanner put close to the plate. Note that the magnitudes of acoustic source strength become smaller than those of the case of the plate discretised into 4 volume velocity sources. The reason for this is that the volume velocity of one source is obtained from the summation of surface velocities multiplied by the area of the rectangular segments enclosed by the boundary of each volume velocity source. Although the results are not shown here, a satisfactory reconstruction was achieved [7] from another experiment using the plate discretised into 6 volume velocities with the 6 appropriately placed microphones to produce a well-conditioned matrix to be inverted.

The foregoing experiments are for the models in which the matrix $\mathbf{H}^H\mathbf{H}$ to be inverted is well-conditioned. What if the conditioning becomes poor? Let us first consider the experimental model depicted in Figure 10. Although this consists of 4 volume velocity sources and 4 microphones, the condition number presented in Figure 11 is much larger (i.e., $7\text{x}10^2$~$6\text{x}10^4$) than that of Figure 5 which also comprises 4 volume velocity sources and 4 microphones. What is more, it is much larger than that of the 16 volume velocity source and 16 microphone model (Figure 8). This poor conditioning results from the improper placement of microphones. That is to say, the microphone array is displaced from the symmetric position in the vertical direction and the microphone-to-microphone distance (0.3m) is chosen differently from the source-to-source distance (0.19m in the horizontal direction and 0.15m in the vertical direction). In addition, the microphone array plane-to-source array plane distance (0.55m) is larger than the source-to-source distance. The consequence of this poor conditioning is a noisy and erroneous reconstruction, as can be seen from Figure 12. In particular, a noticeable discrepancy appears below about 270Hz in the magnitude plots. This is caused by the relatively large condition number at these frequencies compared to that at other frequencies where the overall trend of the inverse reconstruction follows well the directly measured results. Also the phases are reconstructed with deteriorated accuracy. Of course, as could be seen from the

computer simulation results [2], the simple least squares solution is able to restore acoustic source strength extremely well, regardless of the conditioning, if and only if there is no noise in the acoustic pressures and no error in the transfer functions. However, the effect of unwanted error is inevitable.

The next experiment has been performed using 6 microphones instead of 4 microphones for the same plate discretisation as illustrated in Figure 13. Moreover, the microphone array is moved further from the plate (to 1.02m). This enables an investigation of the effect of the worsened conditioning produced by the increase of the source array plane-to-microphone array plane distance. The condition number for this case can be observed from Figure 14 and it is between $3x10^3$~$8x10^5$. That is, comparing this condition number with that of Figure 11, the condition number of $\mathbf{H}^H\mathbf{H}$ is increased by a factor of about 10 by nearly doubling the source array plane-to-microphone array plane distance (the use of two more microphones did not worsen the conditioning [7]). The reason for this can be clearly understood from the behaviour of the condition number of $\mathbf{H}^H\mathbf{H}$ (see reference [1]). As a result of the enlarged condition number, the magnitudes and phases of restored acoustic source strength deviate significantly from the directly measured values (Figure 15).

Now let us reconsider the experimental model comprising 16 volume velocity sources and 16 microphones as presented in Figure 8. From this, as can be seen from Figure 16, we now enlarge the microphone-to-microphone horizontal and vertical distances to 0.2m from 0.075m and 0.095m (Figure 7) and the source array plane-to-microphone array plane distance to 0.661m from 0.046m, but leaving the geometry of microphone array symmetric with respect to the volume velocity source array. Such a positioning of microphones is directed towards increasing the condition number, i.e., $6x10^6$~$1.5x10^9$, as plotted in Figure 17. Note that for Figure 7 the condition number was $5x10$~$3x10^2$. This is because the ratio of the microphone-to-microphone distance to the source-to-source distance is not close to unity (say, 0.2/(0.3/4)=2.7 and 0.2/(0.38/4)=2.1 in the vertical and horizontal direction, respectively) and furthermore the microphone array is positioned far from the plate compared to the source-to-source distance. With this poor conditioning, the simple least squares approach cannot help but restore acoustic source strength very inaccurately. From the overall point of view,

as plotted in Figure 18, the reconstructed magnitudes reveal a biased pattern from the directly measured values, even though the peaks at resonant frequencies can be seen. The restored phases also are in substantial disagreement with the directly measured values.

As observed from the above results, it is easily recognised that the essence of the successful reconstruction of acoustic source strength by the simple least squares method lies on keeping the condition number as small as possible by adjusting the geometrical arrangement of discretised sources and microphones, as long as the experimental environment is sufficient to suppress the strong effect of noise. Also, even though it is not straightforward to express quantitatively the boundary of the large and small condition numbers, a rough guide can be extracted for the case examined here. The above results suggest that if the condition number of the matrix $\mathbf{H}^H\mathbf{H}$ to be inverted is below about 10^3, then the least squares method can provide a satisfactory reconstruction, without using regularisation methods (compare condition numbers shown in Figures 5 and 8 to those plotted in Figures 11, 14 and 17, and the associated results of Figures 6 and 9 to those of Figure 12, 13 and 18). This finding is also consistent with another experiment aimed at the reconstruction of the strengths of two volume velocity sources [7].

6. EXPERIMENTAL RECONSTRUCTION BY TIKHONOV REGULARISATION

Here we discuss how Tikhonov regularisation improves the accuracy of acoustic source strength of the models (Figures 13 and 16) reconstructed poorly by the least squares method alone. For the regularisation parameters, we use β_{qq} which is found by minimising the residual $\|\mathbf{S}_{qq}-\mathbf{S}_{qqR}\|_e$ ($\|\ \|_e$ represents the Euclidean norm of the matrix) between the desired solution $\mathbf{S}_{qq}$ and the Tikhonov regularised solution $\mathbf{S}_{qqR}$, and β_{GCV} which is the minimiser of the generalised cross-validation function $V(\beta)$ [2]. Although the regularisation parameter β_{qq} can be chosen only when having prior knowledge of either the volume velocity or the noise, this is used here as a comparator to check the performance of β_{GCV} which is determined without such prior knowledge.

Tikhonov regularisation is first applied to the experimental model consisting of 4 discretised sources and 6 microphones illustrated in Figure 13. In this case the least

squares approach could not produce a satisfactory reconstruction (Figure 15). For this model, we designed the regularisation parameters β_{qq} and β_{GCV} by following the procedure given by Figures 3 and 4 in reference [2], respectively. The result of Figure 19 compares the two regularisation parameters. They show that the overall trend with frequency is similar to each other, but of course their absolute values are rather different. In this figure, the values at some frequencies (say, about 400~500Hz) indicate that no regularisation is recommended because the volume velocities recovered by the least squares solution at these frequencies are close to the desired values (see Figure 15). The addition of β_{qq} and β_{GCV} into the diagonal components of the original matrix $\mathbf{H}^H\mathbf{H}$ (see equation (4)) improves the conditioning, as graphed in Figure 20. In particular, at frequencies below about 400Hz the matrix becomes better conditioned where the least squares method restored acoustic source strength poorly (see Figure 15). As the result of the improvement of the conditioning from $\kappa(\mathbf{H}^H\mathbf{H})$ to $\kappa(\mathbf{H}^H\mathbf{H}+\beta_{qq}\mathbf{I})$ or $\kappa(\mathbf{H}^H\mathbf{H}+\beta_{GCV}\mathbf{I})$, the Tikhonov regularised solution expressed by equation (4) enhances the accuracy of reconstruction of the magnitudes of volume velocities, as illustrated in Figure 21. As expected, since the values of β_{qq} and β_{GCV} are similar, the acoustic source strengths recovered by use of β_{qq} and β_{GCV} are similar. Reflecting on the fact that β_{GCV} is determined without *a priori* knowledge of either the volume velocity or the noise, we can see that the GCV technique is a practical tool to improve the accuracy of reconstruction of volume velocities. However, as can be seen from Figure 21, Tikhonov regularisation by use of either β_{qq} or β_{GCV} still produces unsatisfactory reconstruction of the phases of the volume velocity cross-spectra between the discretised sources.

The next application of Tikhonov regularisation is performed on the experimental model consisting of the plate discretised into 16 volume velocity sources and 16 microphones as shown in Figure 16. The results shown in Figure 22 compares two regularisation parameters β_{qq} and β_{GCV} chosen by following the steps presented in Figures 3 and 4 in reference [2]. The overall trend is similar in each case, as observed previously. The use of these parameters reduces the original condition number $\kappa(\mathbf{H}^H\mathbf{H})$ into $\kappa(\mathbf{H}^H\mathbf{H}+\beta_{qq}\mathbf{I})$ and $\kappa(\mathbf{H}^H\mathbf{H}+\beta_{GCV}\mathbf{I})$ (approximately 10^{-5} times), as illustrated in Figure 23. The condition numbers of the regularised matrices to be

inverted are below 10^4 up to about 500Hz and below 10^3 beyond this frequency. Recall that for the experimental model having the condition number below 10^3, the least squares solution produced a satisfactory reconstruction (see Figures 4 to 9). With the conditioning improved, the influence of the noise is diminished so effectively that Tikhonov regularised solution using β_{qq} or β_{GCV} reconstructs very remarkably the magnitudes of volume velocities (Figure 24). Note that the magnitudes of volume velocities restored by β_{GCV} are very akin to those recovered by β_{qq}. However, the phase reconstruction is unsatisfactory. Although Figures 21 and 24 present only some of the results, other results which are not shown here revealed similar behaviour.

7.EXPERIMENTAL RECONSTRUCTION BY SINGULAR VALUE DISCARDING

Singular value discarding is now performed for the experimental models to which Tikhonov regularisation has been applied in the previous section. The first application is used with the model of Figure 13 in which the plate is discretised into 4 sources and 6 microphones are employed. Shown in Figure 25 are the singular values of the transfer function matrix $\mathbf{H}$ to be inverted. Their distributions with frequency show clearly why the conditioning of this model is poor at low frequencies (see Figure 14). Note that the dimensions of $\mathbf{H}$ for this model are 6-by-4 and thus there exist 4 singular values. In order to improve the conditioning, we discard some singular values by either the singular value distribution based discarding technique or the generalised cross-validation technique which were discussed in reference [2]. We will denote the matrices containing the singular values left after discarding by the two techniques as $\mathbf{H}_D$ and $\mathbf{H}_v$, respectively. At first, from the singular value distribution presented in Figure 25, the last singular value is removed for frequencies below 400Hz. The reason for choosing this frequency is that as pointed out in section 5, for this model, the least squares method exhibited unsatisfactory reconstruction below this frequency (see Figure 15). As a result, the conditioning of the matrix to be inverted is improved from $\kappa(\mathbf{H})$ to $\kappa(\mathbf{H}_D)$ as illustrated in Figure 26. In this figure, the overlapping of two lines of $\kappa(\mathbf{H})$ and $\kappa(\mathbf{H}_D)$ beyond 400Hz indicates no change of conditioning because no singular value was eradicated. Another elimination of some singular values is made by using the generalised cross-validation function V_v given in reference [2]. The

determination of the singular values to be discarded is made as follows. Firstly, the last diagonal component of the diagonal matrix $\mathbf{I}_\nu$ (see reference [2]) is removed (note that $\mathbf{I}_\nu$ is of dimension 4-by-4 for this model) and the value of the V_ν function is calculated. This calculation is carried out again until two of the last diagonal components of $\mathbf{I}_\nu$ are set to zero. This process is repeated until the third to last diagonal components of $\mathbf{I}_\nu$ are replaced by zero. Of the calculated values of the V_ν function, we select the minimum value. At this point, if the associated $\mathbf{I}_\nu$ producing the minimum V_ν has ν unities from the 1st to the νth element on its diagonal, then the $(\nu+1)$th to 4th singular values of the matrix $\mathbf{H}$ (m-by-n, $m \geq n$) are truncated. Thus, the matrix $\mathbf{H}$ is transformed into $\mathbf{H}_\nu$. This is repeated at each component of frequency to be analysed. Figure 26 compares $\kappa(\mathbf{H}_\nu)$ with $\kappa(\mathbf{H}_D)$ and shows that $\kappa(\mathbf{H}_\nu)$ follows $\kappa(\mathbf{H}_D)$ well, except beyond 400Hz. In this figure, $\kappa(\mathbf{H}_\nu)=\kappa(\mathbf{H}_D)$ at many frequencies signifies that the minimum value of V_ν at those frequencies is achieved by removing only the last (here the 4th) singular value (because $\kappa(\mathbf{H}_D)$ was obtained after discarding the last singular value up to 400Hz). The results of Figure 27 show some of the reconstructed volume velocities. The magnitudes of volume velocities recovered by using $\mathbf{H}_D$ and $\mathbf{H}_\nu$ approach the desired values very closely, compared to those achieved by the simple least squares method. Furthermore, since the levels of conditioning are similar, these two reconstructed results are similar. In contrast with the magnitude reconstruction, the restored phases show unsatisfactory results. In the meantime, comparing the results of Figure 27 with Figure 21 reveals that the accuracy of reconstruction by singular value discarding is similar to that given by Tikhonov regularisation.

Now we will consider the experimental model given by Figure 16 which consists of the plate discretised into 16 sources and 16 microphones. For this model, a plot of the distribution of 16 singular values is presented in Figure 28. As in the previous case, the choice of singular values to be discarded is made by two methods based on the singular value distribution and generalised cross-validation function. Based on the singular value distribution of Figure 28, we first partition the frequency of interest, 90-1000Hz, into 3 zones: frequencies < 500Hz, 500Hz ≤ frequencies ≤

600Hz, and frequencies > 600Hz. For each zone, the singular values less than $1x10^2$, $2x10^2$, and $3x10^2$ are truncated. Note that these values are chosen arbitrarily based on empirical experience. As a result, the conditioning $\kappa(\mathbf{H})$ of the original matrix $\mathbf{H}$ to be inverted is enhanced by $\kappa(\mathbf{H}_D)$ as plotted in Figure 29. Elimination of some singular values by using generalised cross-validation is performed as in the previous case. However, since the dimension of $\mathbf{I}_v$ of this model is 16-by-16, the calculation of the V_v function is repeated until the 3rd to 16th diagonal components of $\mathbf{I}_v$ are replaced by zero. Plotted in Figure 29 is the condition number of the matrix $\mathbf{H}_v$. Unlike the previous case of Figure 26, $\kappa(\mathbf{H}_v)$ is mostly different from $\kappa(\mathbf{H}_D)$ and shows a noisy pattern. The results of Figure 30 illustrate that the use of the singular value discarded matrix $\mathbf{H}_D$ instead of the original matrix $\mathbf{H}$ improves the accuracy of reconstruction of the magnitudes of volume velocities which were restored badly by the simple least squares method alone. In contrast with this the use of $\mathbf{H}_v$ reconstructs the magnitudes of volume velocities unsatisfactorily, revealing a noisy shape. Needless to say, this is in connection with $\kappa(\mathbf{H}_v)$ having a noisy pattern, which indicates that for this model singular value discarding by minimising the generalised cross-validation function does not appear to work satisfactorily. For this model the phase recovery by both $\mathbf{H}_D$ and $\mathbf{H}_v$ is poor.

From the experimental reconstruction results presented in sections 6 and 7, it has been observed that the application of Tikhonov regularisation or singular value discarding to an ill-conditioned system can provide considerable improvement in accuracy of reconstruction, which was also illustrated from simulation results presented in reference [2]. Also, the GCV technique has been seen to be a practical tool for choosing properly the regularisation parameter and the singular values to be truncated. However, stress should be laid on the fact that the GCV technique does not always lead to a successful choice of those values. As could be seen, the GCV technique has chosen appropriately the regularisation parameters and the singular values to be eliminated for most of the experimental models considered up to now. However, this had not decided properly the singular values to be eliminated for the 16 source and 16 microphone model. Accordingly, in applying the GCV technique, we have to recall the cautionary remarks given in reference [2].

8. CONCLUSIONS

Through a series of experiments using various models, the least squares method has been shown to be capable of reconstructing the volume velocities of a randomly vibrating simply supported plate with good accuracy, when the conditioning of the matrix to be inverted is made small. Although it is in general not straightforward to judge the boundary between "small" and "large" condition numbers, the experimental results presented here suggested that the condition number of the matrix $\mathbf{H}^{H}\mathbf{H}$ can be said to be small when this is below about 10^3. Tikhonov regularisation using β_{GCV} which is chosen by minimising the generalised cross-validation function improves considerably the poor accuracy of volume velocities reconstructed by the least squares method alone. These results have shown a similar trend to those reconstructed by using β_{qq} which is used as comparator to check the performance of β_{GCV} and is determined by minimising the difference between the desired and estimated volume velocities. However, the regularisation parameters β_{qq} and β_{GCV} have also shown unsatisfactory performance in improving the phases of volume velocity cross-spectra reconstructed poorly by the least squares method alone. Singular value discarding based on the singular value distribution has shown that the volume velocity distributions and their interactions can be reconstructed more approximately, compared to the values obtained by only the simple least squares method. On the contrary, singular value discarding using the generalised cross-validation technique has revealed a model dependent performance. This is thought to be a limitation of the generalised cross-validation technique, which has been already pointed out by some researchers [2].

ACKNOWLEDGEMENT

This research was financially supported by the Daewoo Motor Company, Korea.

REFERENCES

1. P. A. NELSON and S. H. YOON 1998 *ISVR Technical Report No. 278, University of Southampton.* Estimation of acoustic source strength by inverse methods: Part I, Conditioning of the inverse problem.
2. S. H. YOON and P. A. NELSON 1998 *ISVR Technical Report No. 279, University of Southampton.* Estimation of acoustic source strength by inverse methods: Part II, Methods for choosing regularisation parameters.
3. S. H. YOON 1998 *PhD Thesis, University of Southampton.* Reconstruction of acoustic source strength distributions and their interactions by inverse techniques.
4. NATIONAL INSTRUMENT 1996 *Instrumentation reference and catalogue.*
5. R. D. BREVINS 1979 *Formulas for natural frequency and mode shape.* Van Nostrand Reinhold Company.
6. N. A. HALLIWELL 1979 *Journal of Sound and Vibration* **62**, 312-315. Laser-doppler measurement of vibrating surfaces: a portable instrument.
7. K. R. HOLLAND and F. J. FAHY 1996 *Proceedings InterNoise* **96**, 2581-2584. Application of an area-integrating vibration velocity transducer.

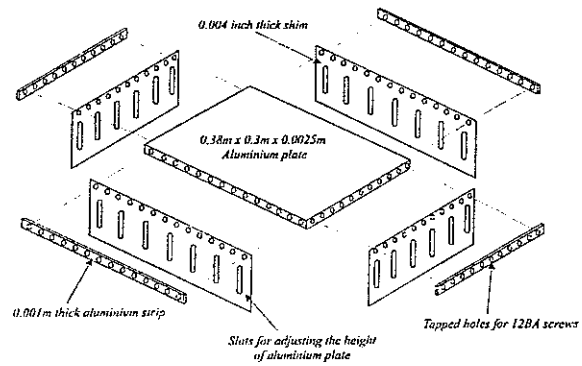
0.004 inch thick shim
0.38m x 0.3m x 0.0025m
Aluminium plate
0.001m thick aluminium strip
Slots for adjusting the height
of aluminium plate
Tapped holes for 12BA screws

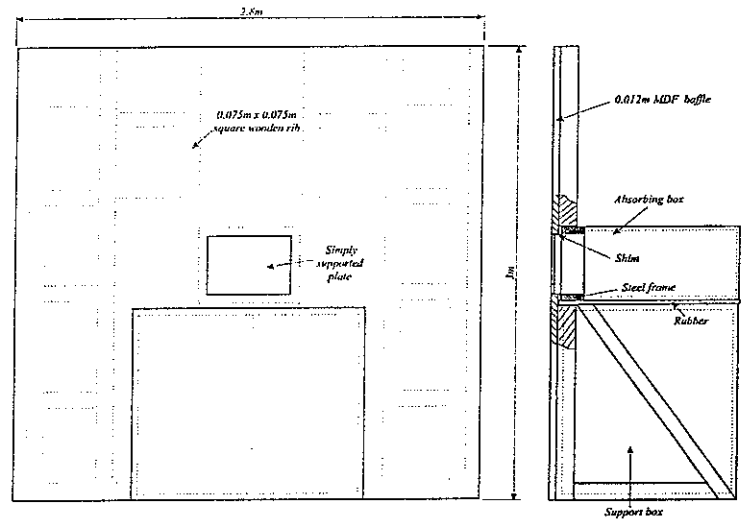
2.8m
3m
0.075m x 0.075m
square wooden rib
Simply
supported
plate
0.012m MDF baffle
Absorbing box
Shim
Steel frame
Rubber
Support box

Figure 1

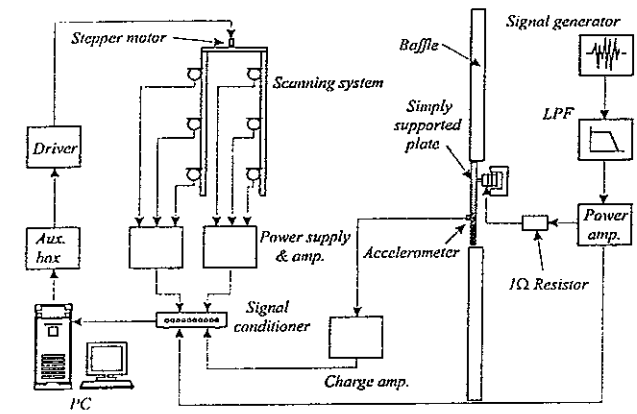
Stepper motor
Scanning system
Driver
Aux. box
Power supply & amp.
Signal conditioner
PC
Charge amp.
Baffle
Signal generator
Simply supported plate
LPF
Power amp.
Accelerometer
1Ω Resistor

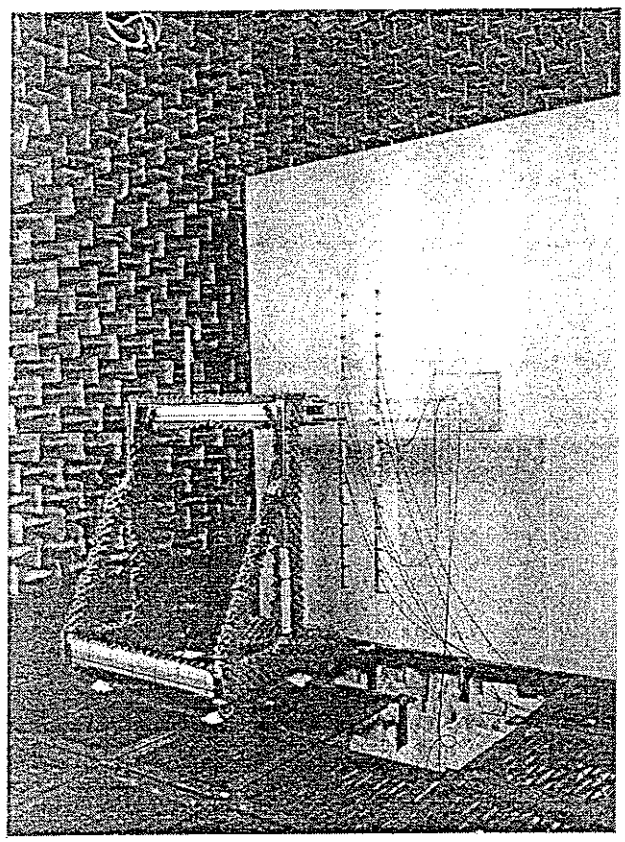

Figure 2

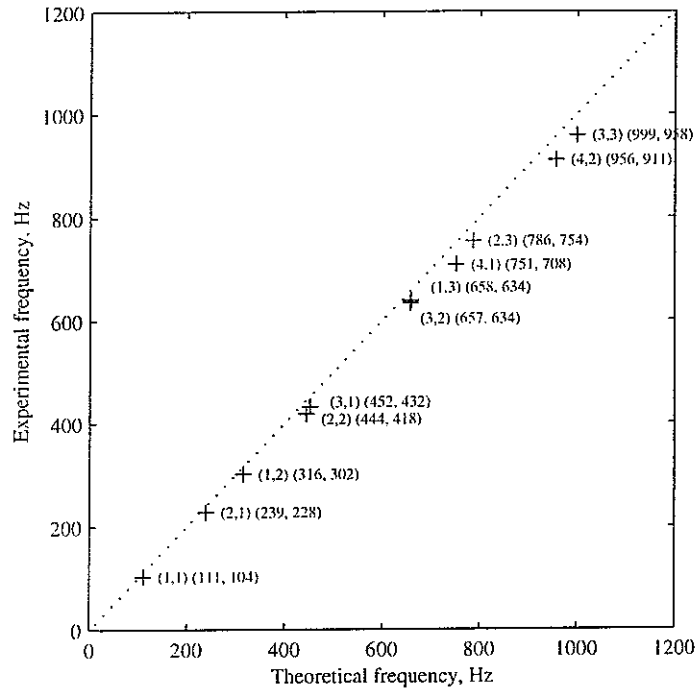

Figure 3. A comparison of the theoretical and experimental natural frequencies of the simply supported plate. Figures in the 1st parenthesis denote the modal indices, and those in the 2nd parenthesis the theoretical and experimental natural frequencies, respectively.

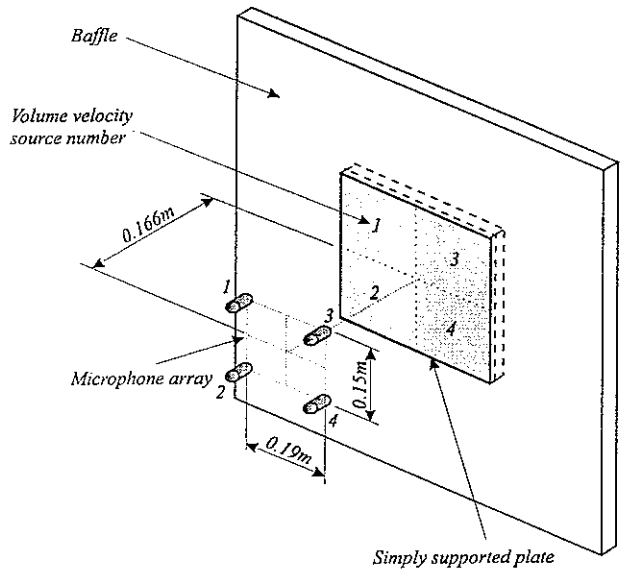

Figure 4. A geometrical arrangement of the plate system discretised into 4 volume velocity sources and 4 microphones.

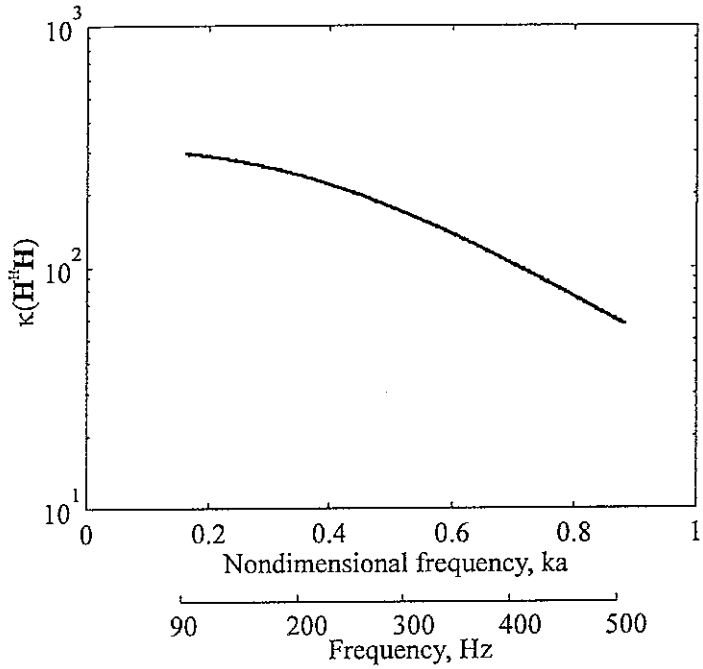

Figure 5. Condition number $\kappa(\mathbf{H}^H\mathbf{H})$ of the model of Figure 4.

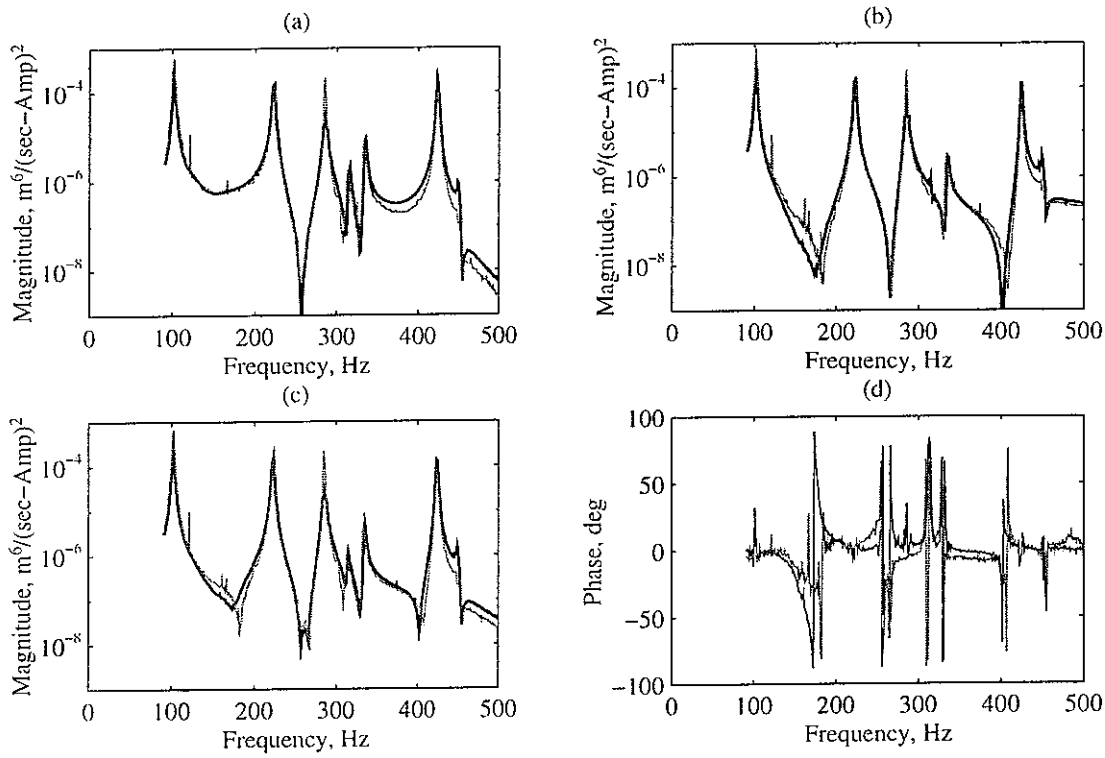

Figure 6. A comparison of the directly measured (black) and reconstructed (by the least squares solution, grey) volume velocity (per unit ampere) auto-spectra of sources (a) 2, (b) 3 and cross-spectra between sources 2 and 3 ((c) magnitude, (d) phase) for the model of Figure 4.

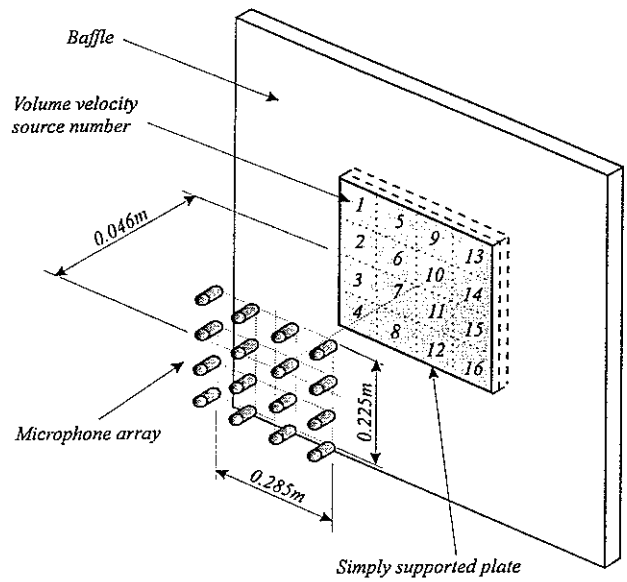

Figure 7. A geometrical arrangement of the plate system discretised into 16 volume velocity sources and 16 microphones.

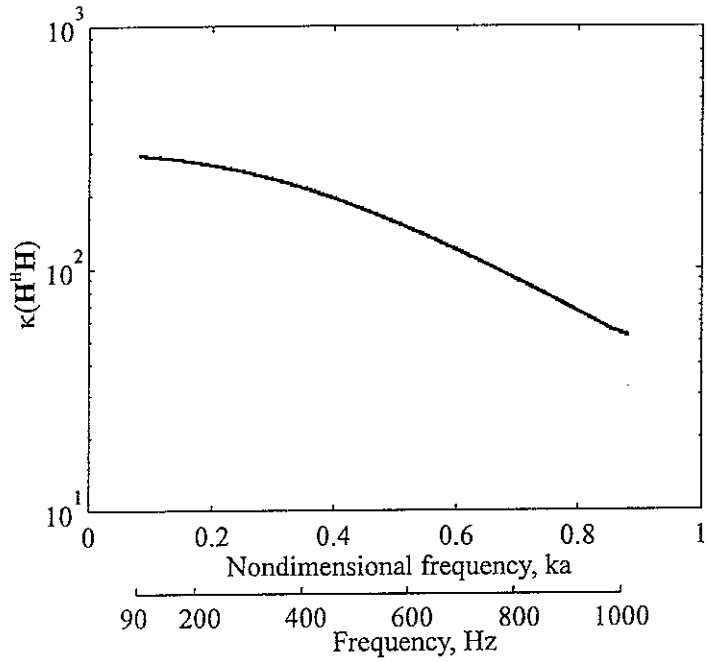

Figure 8. Condition number $\kappa(\mathbf{H}^H\mathbf{H})$ of the model of Figure 7.

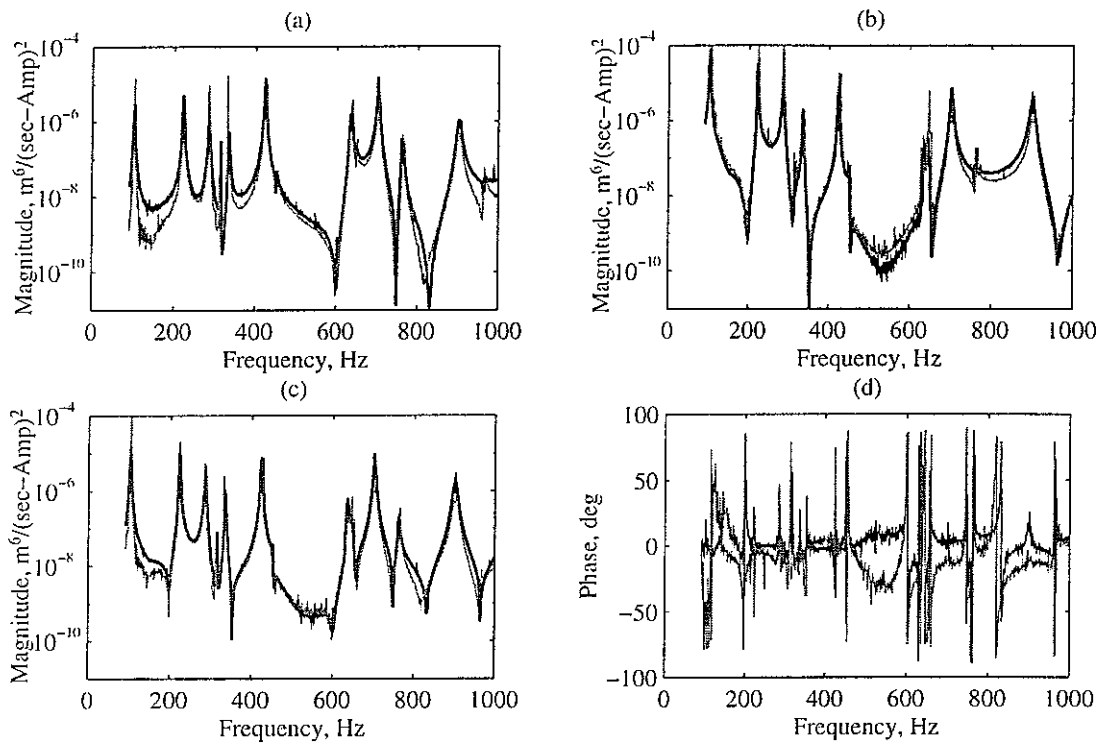

Figure 9. A comparison of the directly measured (black) and reconstructed (by the simple least squares solution, grey) volume velocity (per unit ampere) auto-spectra of sources (a) 1, (b) 11 and cross-spectra between sources 1 and 11 ((c) magnitude, (d) phase) for the model of Figure 7.

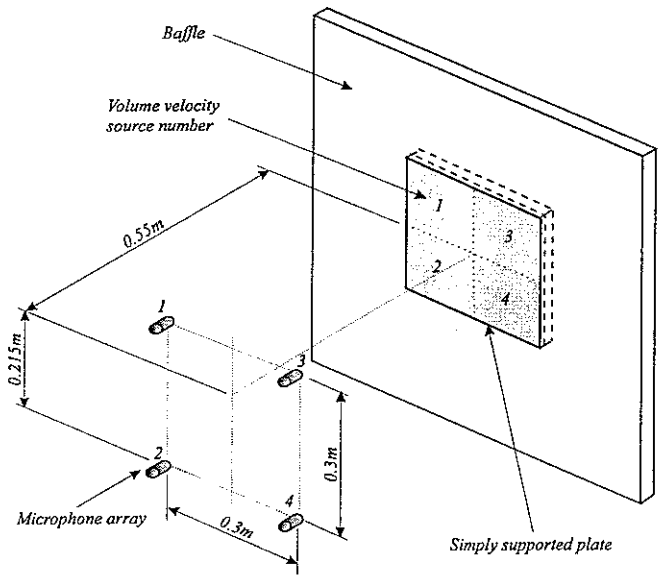

Figure 10. A geometrical arrangement of the plate system discretised into 4 volume velocity sources and 4 microphones.

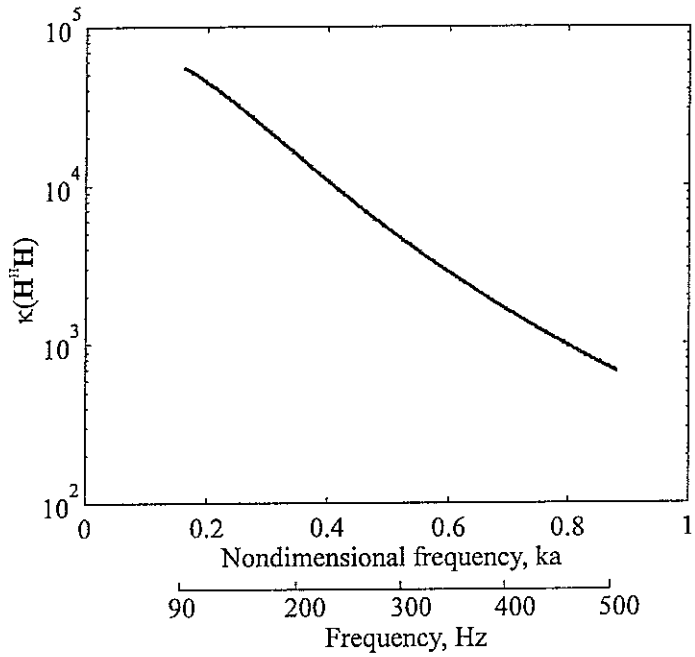

Figure 11. Condition number $\kappa(\mathbf{H}^H\mathbf{H})$ of the model of Figure 10.

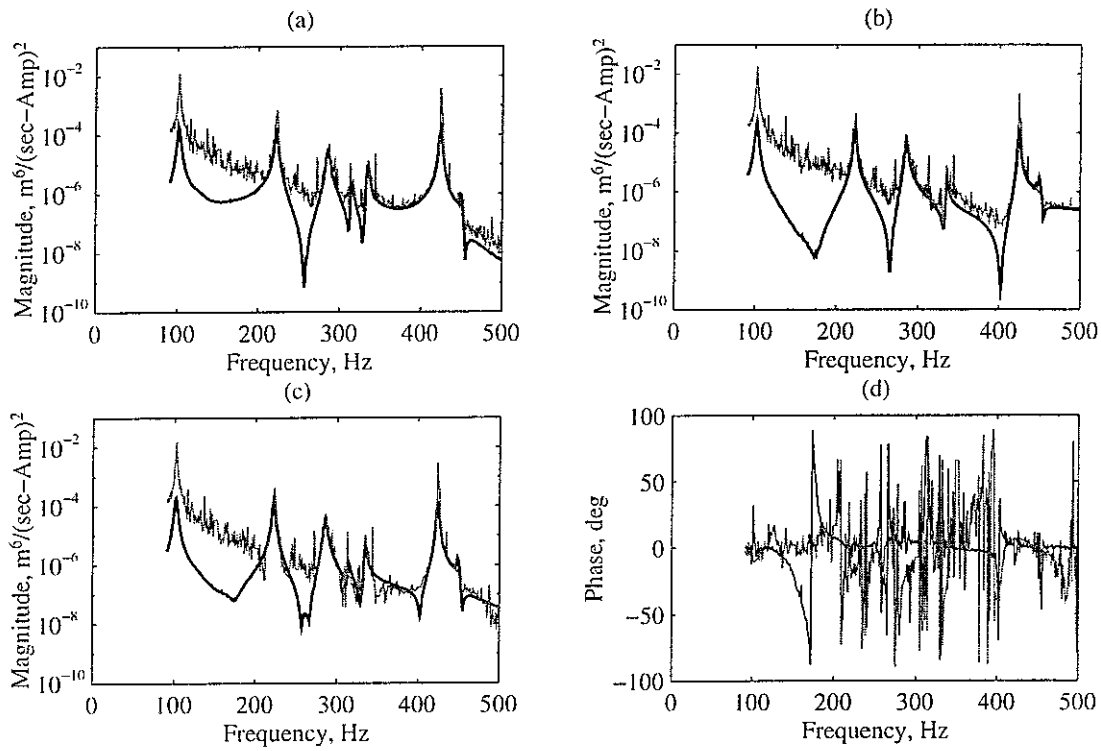

Figure 12. A comparison of the directly measured (black) and reconstructed (by the least squares solution, grey) volume velocity (per unit ampere) auto-spectra of sources (a) 2, (b) 3 and cross-spectra between sources 2 and 3 ((c) magnitude, (d) phase) for the model of Figure 10.

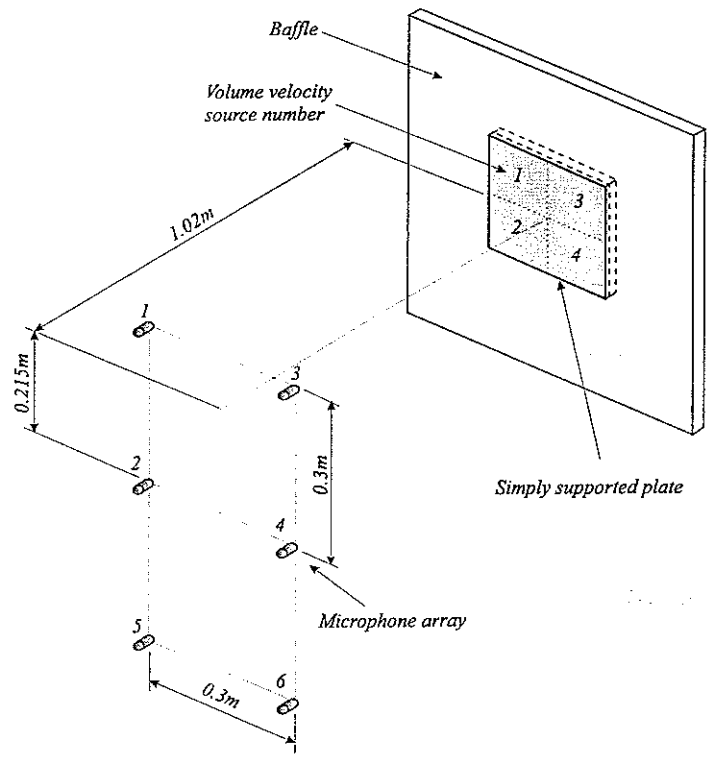

Figure 13. A geometrical arrangement of the plate system discretised into 4 volume velocity sources and 6 microphones.

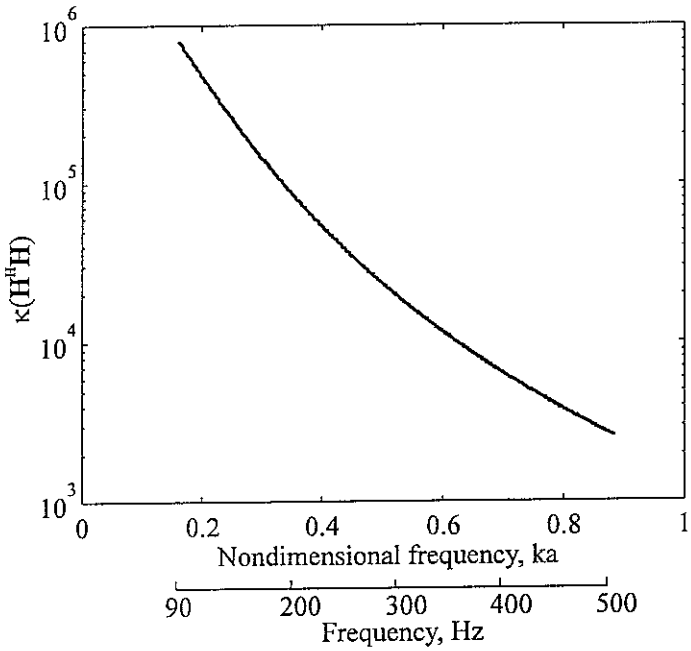

Figure 14. Condition number $\kappa(\mathbf{H}^H\mathbf{H})$ of the model of Figure 13.

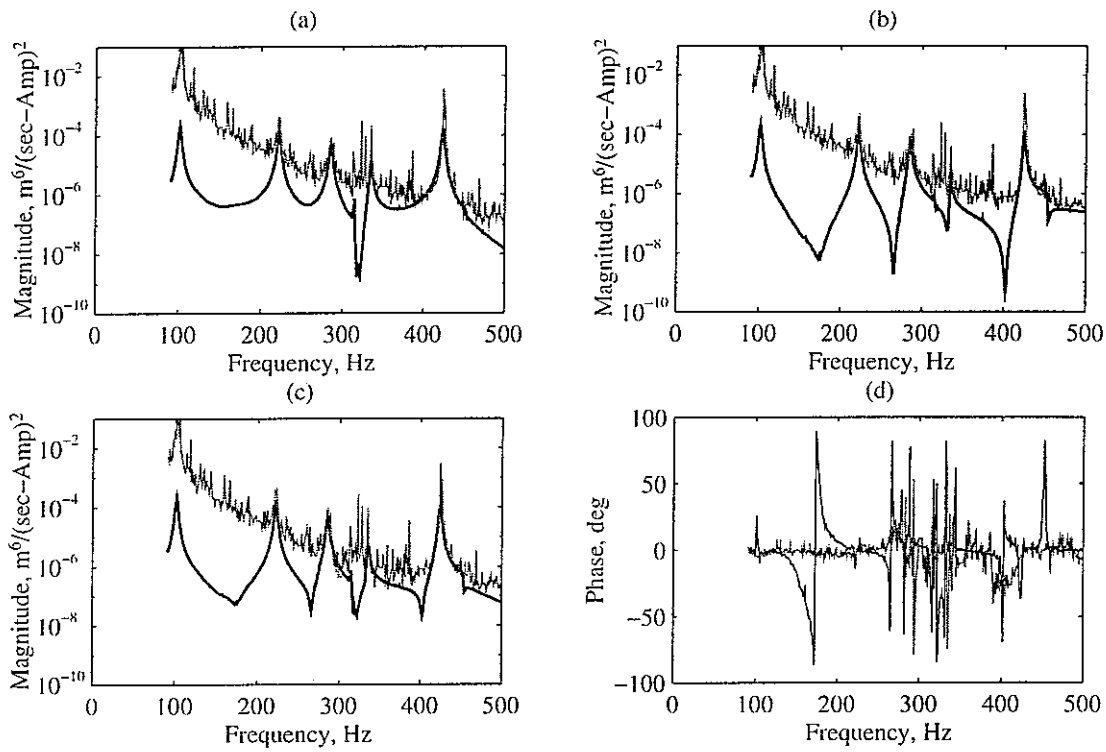

Figure 15. A comparison of the directly measured (black) and reconstructed (by the least squares solution, grey) volume velocity (per unit ampere) auto-spectra of sources (a) 1, (b) 3 and cross-spectra between sources 1 and 3 ((c) magnitude, (d) phase) for the model of Figure 13.

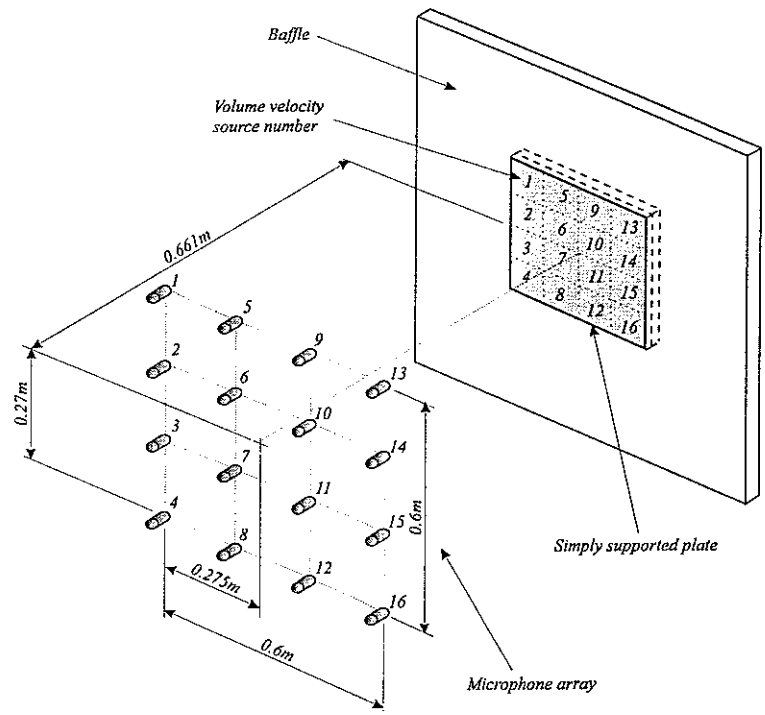

Figure 16. A geometrical arrangement of the plate system discretised into 16 volume velocity sources and 16 microphones.

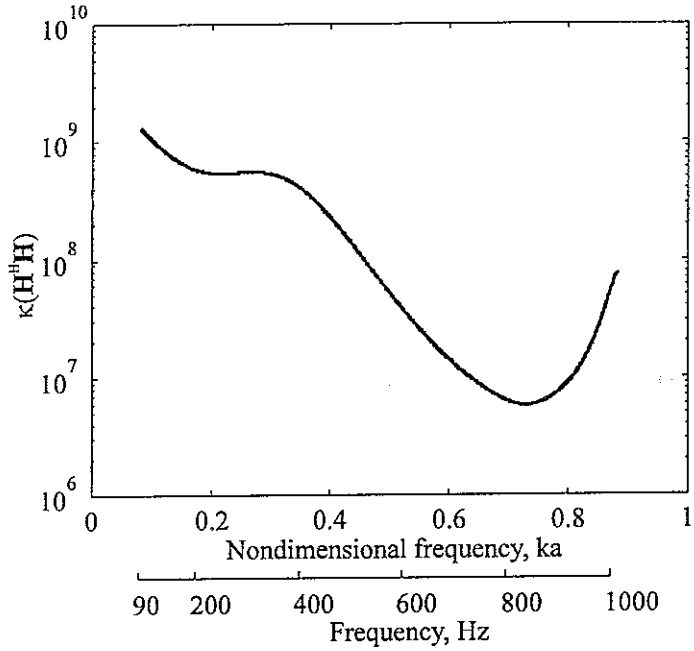

Figure 17. Condition number $\kappa(\mathbf{H}^{H}\mathbf{H})$ of the model of Figure 16.

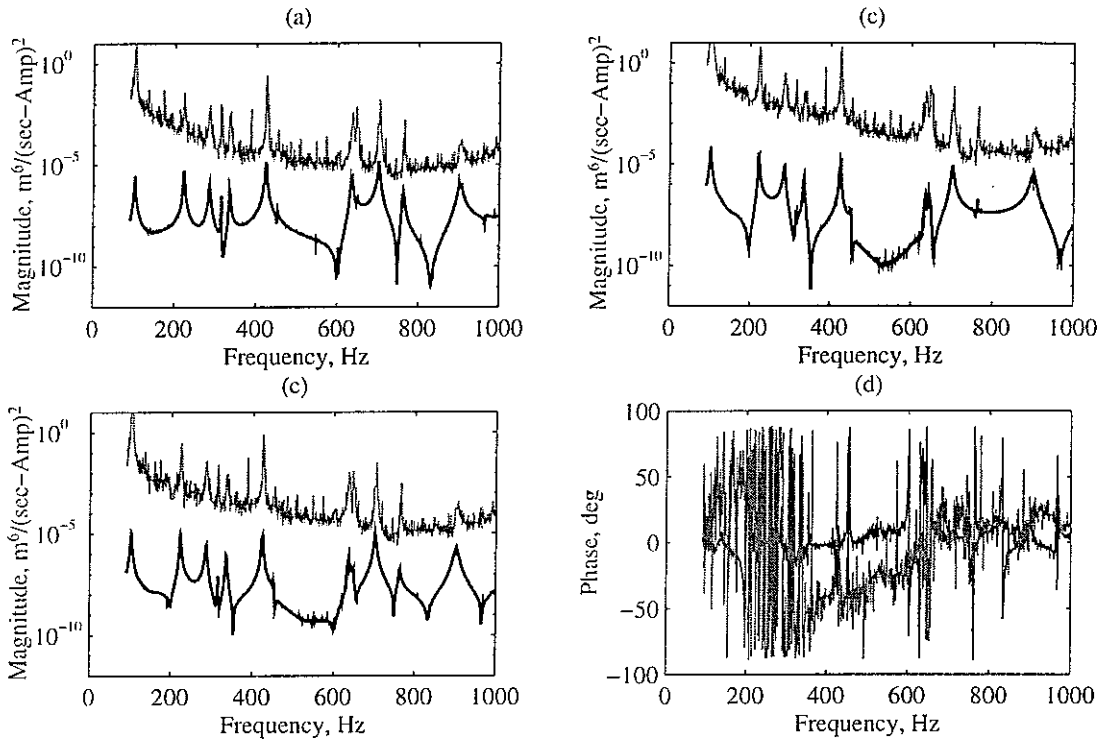

Figure 18. A comparison of the directly measured (black) and reconstructed (by the simple least squares solution, grey) volume velocity (per unit ampere) auto-spectra of sources (a) 1, (b) 11 and cross-spectra between sources 1 and 11 ((c) magnitude, (d) phase) for the model of Figure 16.

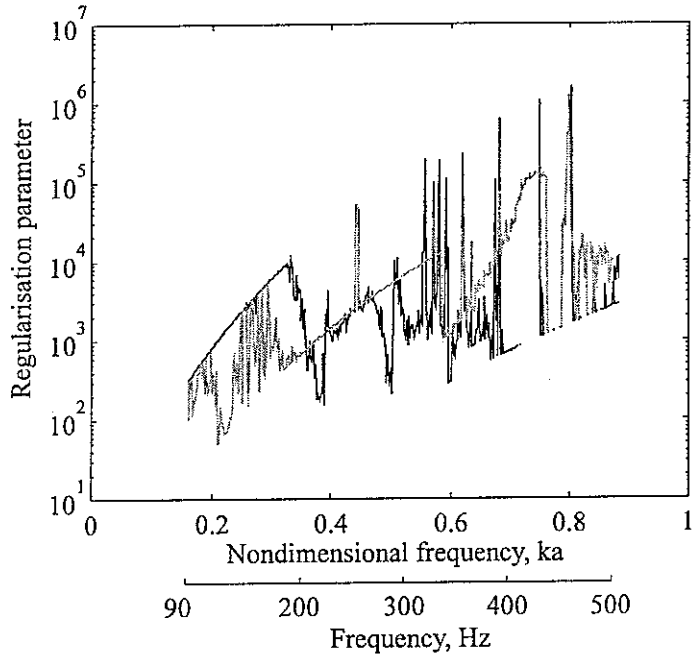

Figure 19. Regularisation parameters for the model of Figure 13: β_{qq} (black) and β_{GCV} (grey). $a=L_x/4$, $L_x=0.38$m.

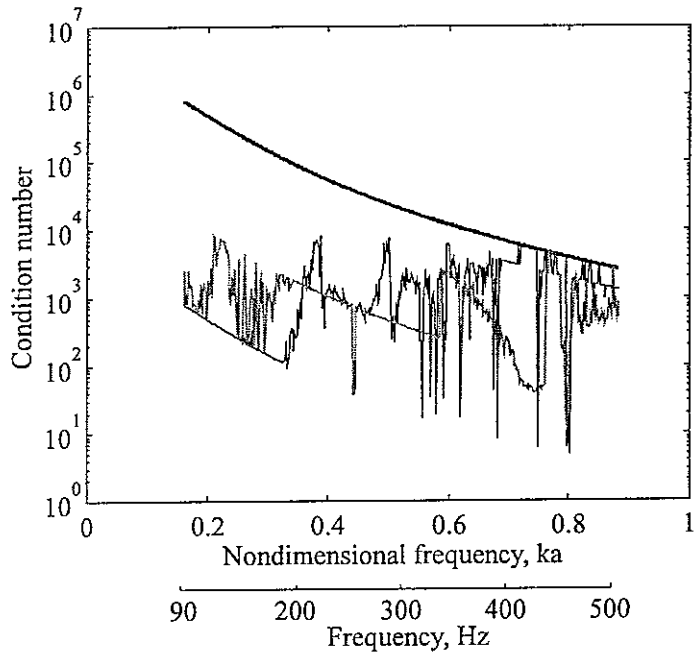

Figure 20. Condition numbers for the model of Figure 13: $\kappa(\mathbf{H}^H\mathbf{H})$ (thick black), $\kappa(\mathbf{H}^H\mathbf{H}+\beta_{qq}\mathbf{I})$ (thin black) and $\kappa(\mathbf{H}^H\mathbf{H}+\beta_{GCV}\mathbf{I})$ (grey). $a=L_x/4$, $L_x=0.38$m.

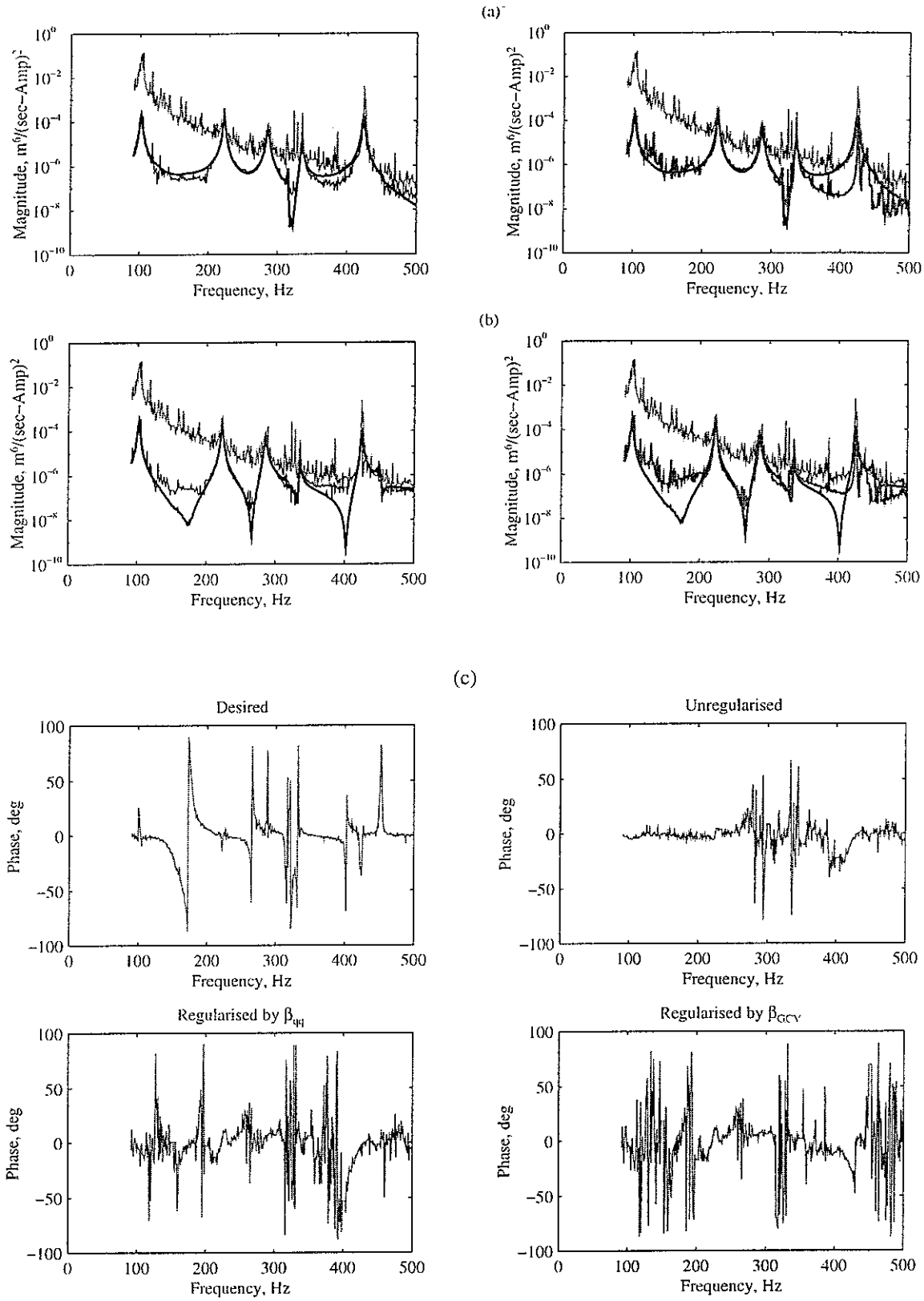

Figure 21. Volume velocity (per unit ampere) auto-spectra of sources (a) 1, (b) 3: desired (thick black), unregularised (thin grey), regularised by β_{qq} (thin black), regularised by β_{GCV} (thick grey). (c) Phase of cross-spectra between sources 1 and 3 for the model of Figure 13.

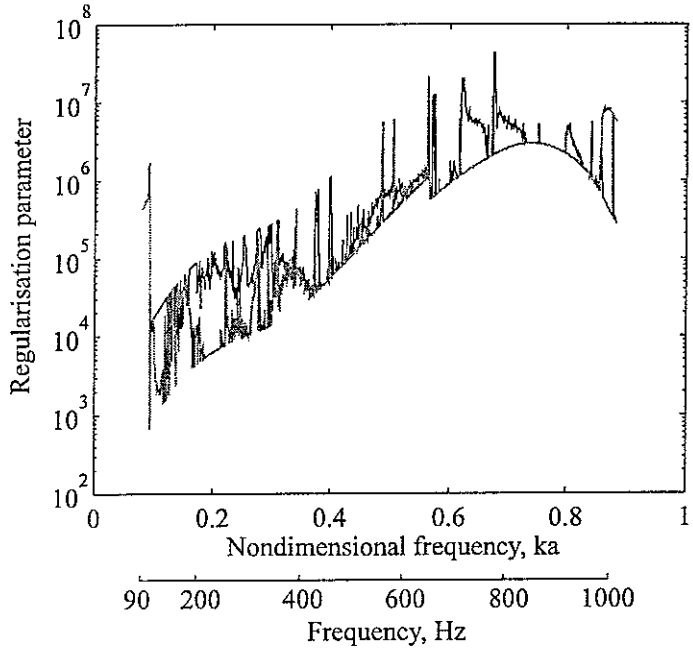

Figure 22. Regularisation parameters for the model of Figure 16: β_{qq} (black) and β_{GCV} (grey). $a=L_x/8$, $L_x=0.38$m.

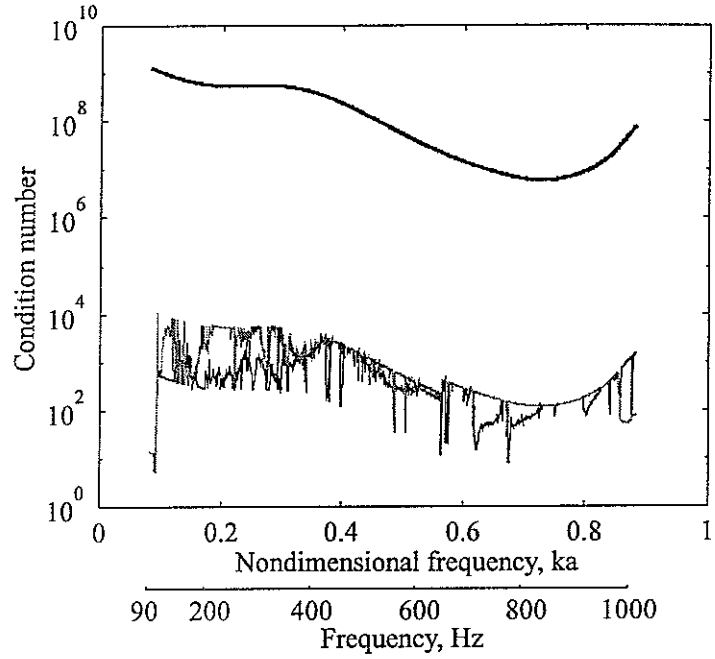

Figure 23. Condition numbers for the model of Figure 16: $\kappa(\mathbf{H}^{\mathrm{H}}\mathbf{H})$ (thick black), $\kappa(\mathbf{H}^{\mathrm{H}}\mathbf{H}+\beta_{qq}\mathbf{I})$ (thin black) and $\kappa(\mathbf{H}^{\mathrm{H}}\mathbf{H}+\beta_{\mathrm{GCV}}\mathbf{I})$ (grey). $a=L_x/8$, $L_x=0.38$m.

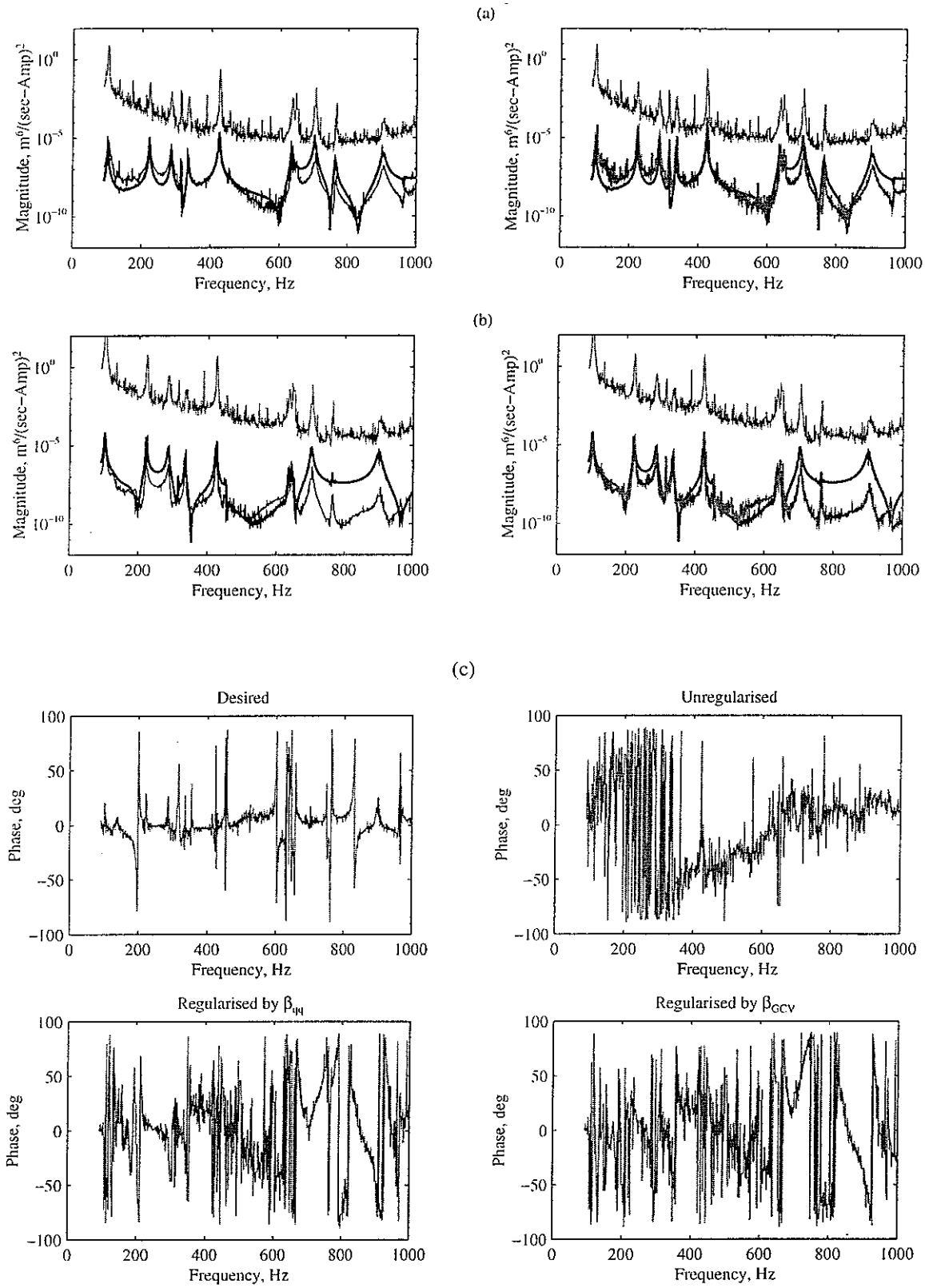

Figure 24. Volume velocity (per unit ampere) auto-spectra of sources (a) 1, (b) 11: desired (thick black), unregularised (thin grey), regularised by β_{qq} (thin black), regularised by β_{GCV} (thick grey). (c) Phase of cross-spectra between sources 1 and 11 for the model of Figure 16.

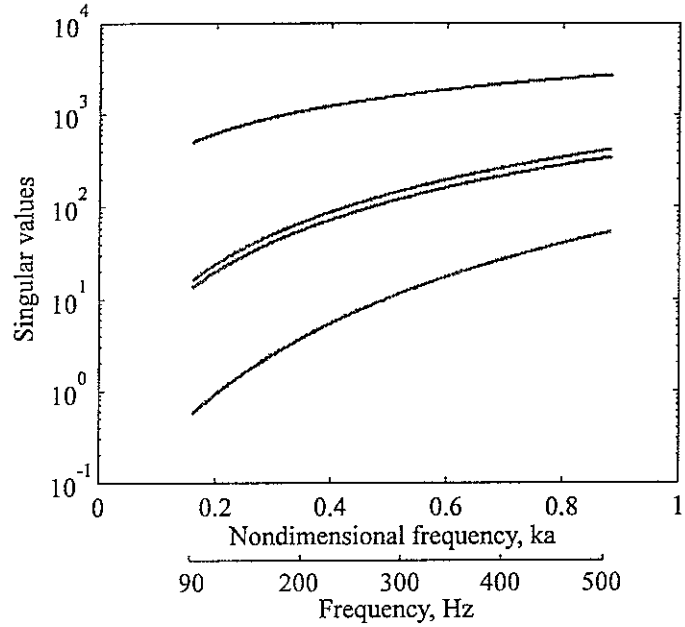

Figure 25. Singular values of the matrix **H** for the model of Figure 13. $a=L_x/4$, L_x=0.38m.

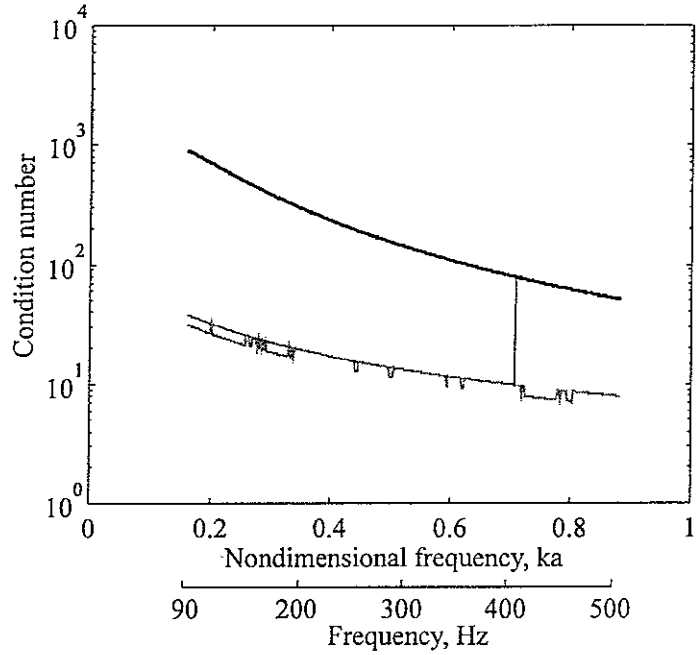

Figure 26. Condition numbers for the model of Figure 13: $\kappa(\mathbf{H})$ (thick black), $\kappa(\mathbf{H}_D)$ (thin black) and $\kappa(\mathbf{H}_v)$ (grey). $a=L_x/4$, L_x=0.38m.

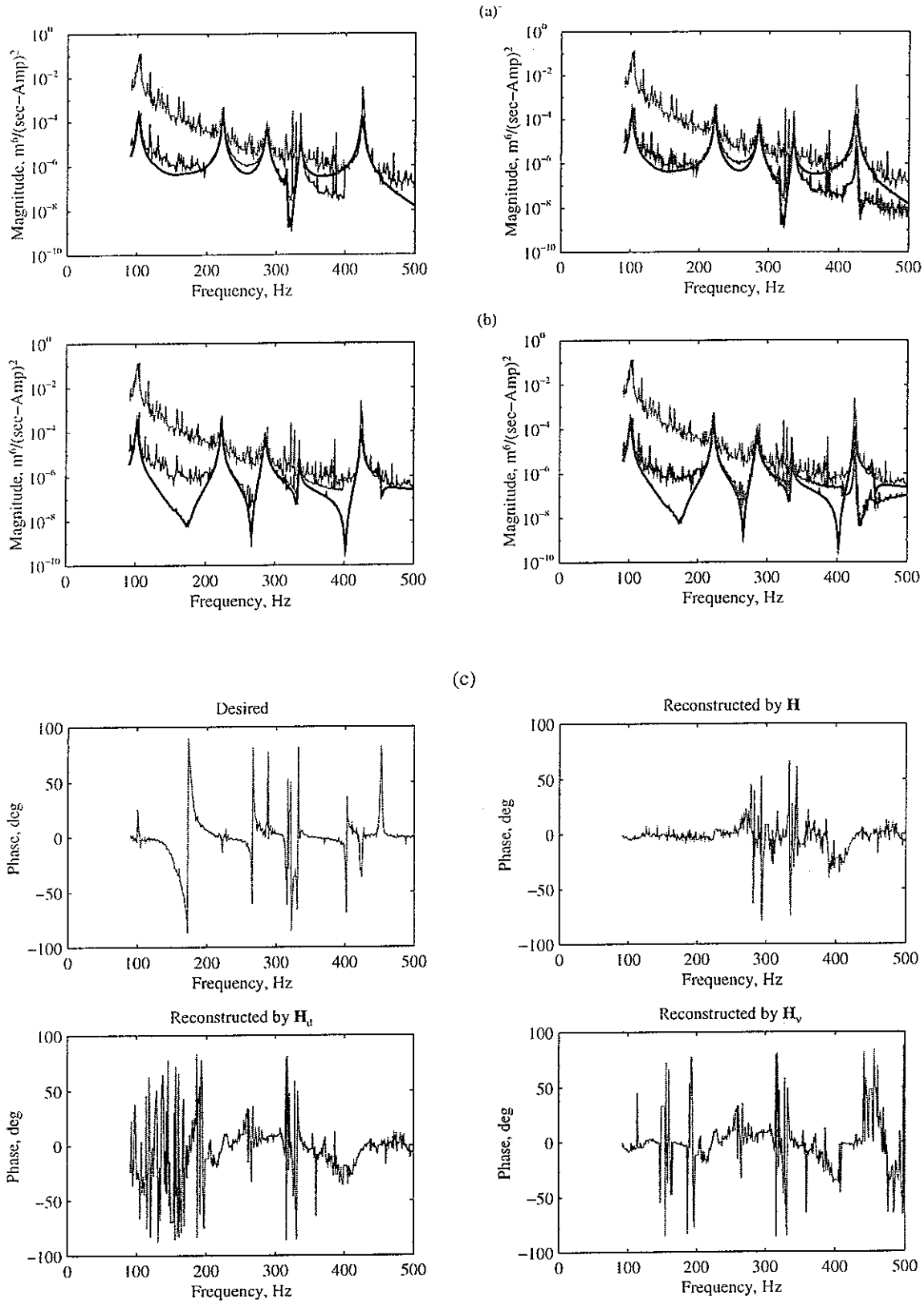

Figure 27. Volume velocity (per unit ampere) auto-spectra of sources (a) 1, (b) 3: desired (thick black), undiscarded (thin grey), reconstructed by $\mathbf{H}_D$ (thin black), reconstructed by $\mathbf{H}_v$ (thick grey). (c) Phase of cross-spectra between sources 1 and 3 for the model of Figure 13.

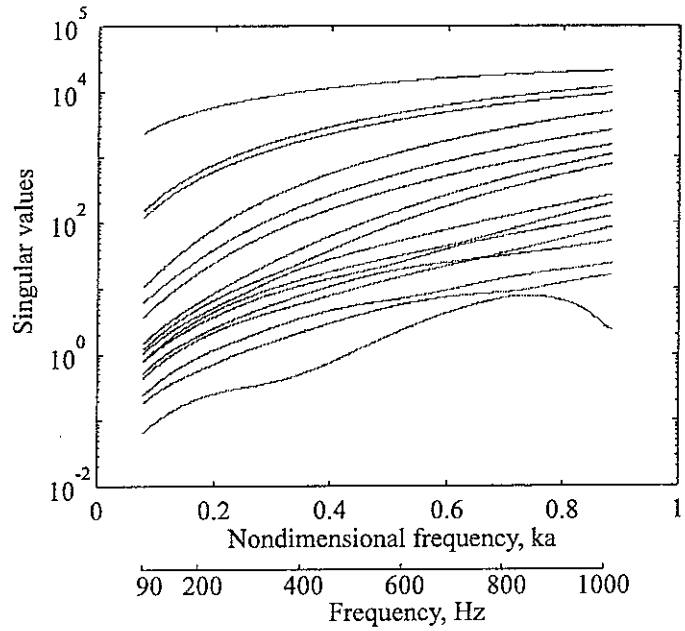

Figure 28. Singular values of the matrix **H** for the model of Figure 16. $a=L_x/8$, L_x=0.38m.

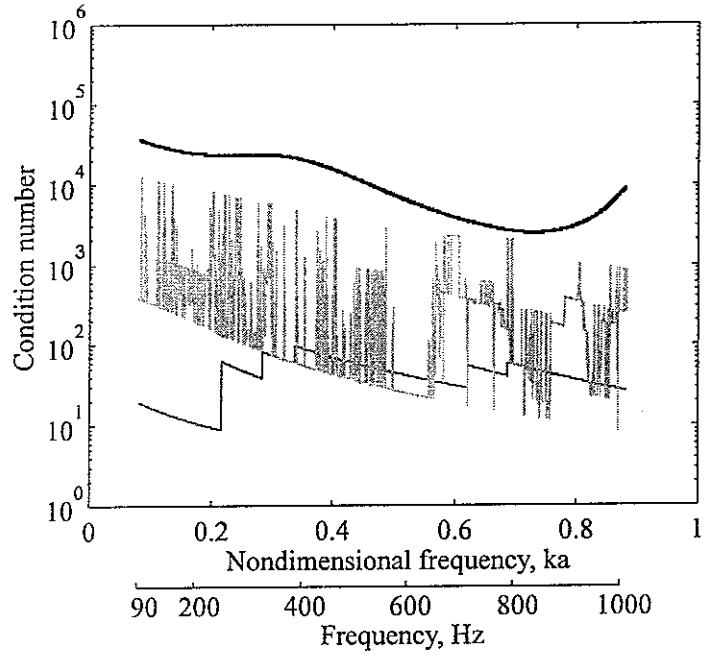

Figure 29. Condition numbers for the model of Figure 16: $\kappa(\mathbf{H})$ (thick black), $\kappa(\mathbf{H}_D)$ (thin black) and $\kappa(\mathbf{H}_v)$ (grey). $a=L_x/8$, L_x=0.38m.

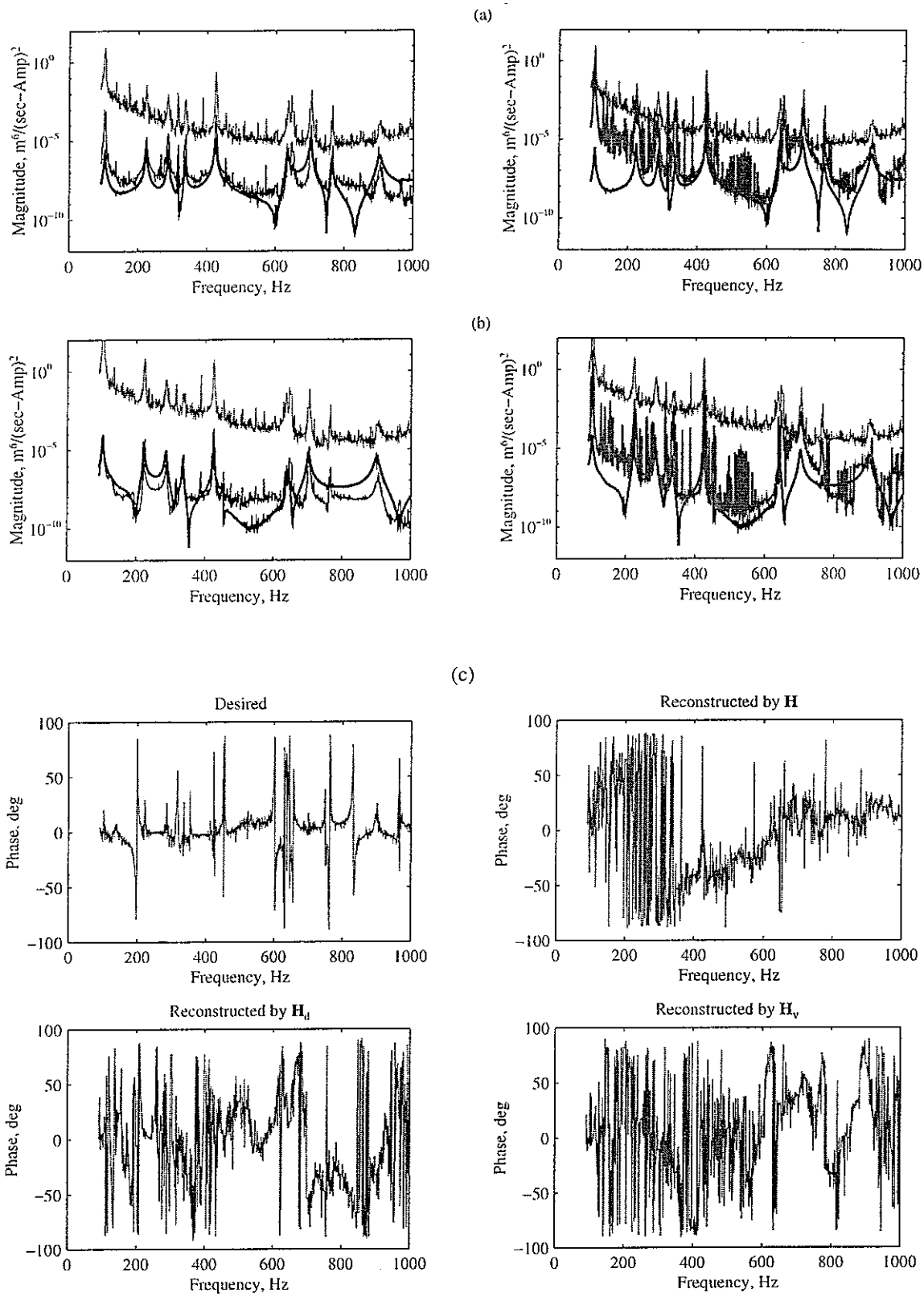

Figure 30. Volume velocity (per unit ampere) auto-spectra of sources (a) 1, (b) 11: desired (thick black), undiscarded (thin grey), reconstructed by $\mathbf{H}_D$ (thin black), reconstructed by $\mathbf{H}_v$ (thick grey). (c) Phase of cross-spectra between sources 1 and 11 for the model of Figure 16.